Journal Pre-proof

A thiol redox sensor in soluble epoxide hydrolase enables oxidative activation by intra-protein disulfide bond formation

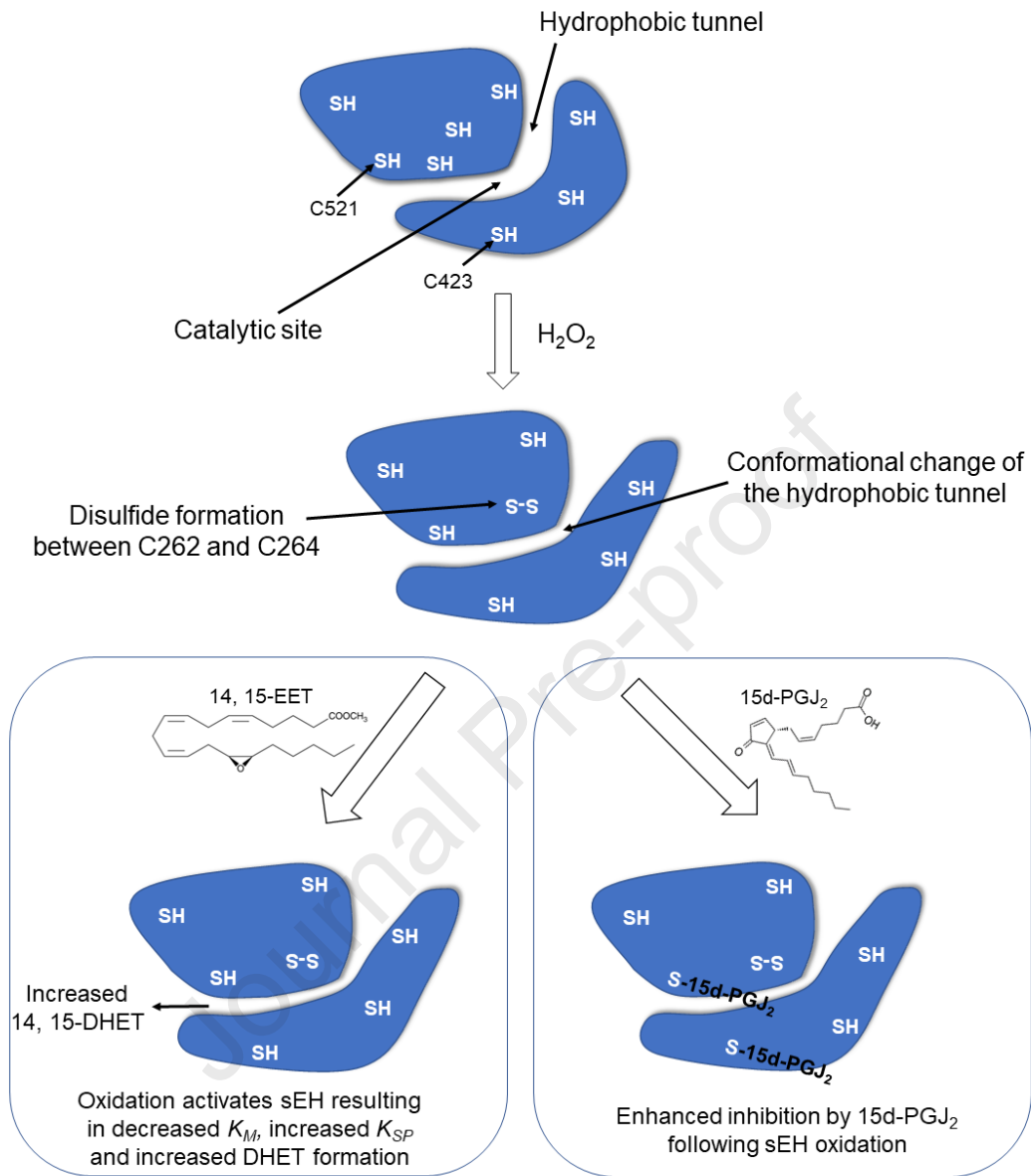Rebecca L. Charles, Giancarlo Abis, Beatriz F. Fernandez, Sebastian Guttzeit, Roberto Buccafusca, Maria R. Conte, Philip Eaton

Please cite this article as: R.L. Charles, G. Abis, B.F. Fernandez, S. Guttzeit, R. Buccafusca, M.R. Conte, P. Eaton, A thiol redox sensor in soluble epoxide hydrolase enables oxidative activation by intra-protein disulfide bond formation, *Redox Biology* (2021), doi: https://doi.org/10.1016/j.redox.2021.102107.

This is a PDF file of an article that has undergone enhancements after acceptance, such as the addition of a cover page and metadata, and formatting for readability, but it is not yet the definitive version of record. This version will undergo additional copyediting, typesetting and review before it is published in its final form, but we are providing this version to give early visibility of the article. Please note that, during the production process, errors may be discovered which could affect the content, and all legal disclaimers that apply to the journal pertain.
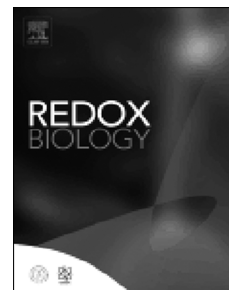
A thiol redox sensor in soluble epoxide hydrolase enables oxidative activation by intra-protein disulfide bond formation.

Rebecca L Charles[a, 1], Giancarlo Abis [b, i, 1], Beatriz F Fernandez[c], Sebastian Guttzeit[c], Roberto Buccafusca[d], Maria R Conte[b,*], Philip Eaton[a,*].

  a. Queen Mary University of London, William Harvey Research Institute, Charterhouse Square, London, EC1M 6BQ.
  b. King's College London, Randall Centre for Cell and Molecular Biophysics, School of Basic and Medical Biosciences, London, SE1 1UL.
  c. King's College London, The British Heart Foundation Centre of Excellence, The Rayne Institute, St Thomas' Hospital, London, SE1 7EH.
  d. Queen Mary University of London, School of Biological and Chemical Sciences, Mile End Road, London, E1 4NS.

[1] R.L.C. and G.A. contributed equally to this work

[i] Current address: Division of Bioscience, Institute of Structural and Molecular Biology, University College London, Darwin Building, Gower Street, London, WC1E 6BT.

* Correspondence should be addressed to:

Philip Eaton,
Queen Mary University of London,
William Harvey Research Institute,
Charterhouse Square,
London,
EC1M 6BQ.
Email: p.eaton@qmul.ac.uk

Sasi Conte (Maria R Conte),
King's College London,
Randall Centre for Cell and Molecular Biophysics,
School of Basic and Medical Biosciences,
London,
SE1 1UL.
Email: sasi.conte@kcl.ac.uk

Author Contributions: R.L.C., G.A., M.R.C., and P.E. designed research; R.L.C., G.A., B.F.F., S.G., and R.B. performed research; R.L.C., G.A., B.F.F., S.G., R.B., M.R.C., and P.E. analyzed data; R.L.C., G.A., M.R.C., and P.E. wrote the paper.

This PDF file includes:

Main Text

Figures 1 to 5

Abstract

Soluble epoxide hydrolase (sEH), an enzyme that broadly regulates the cardiovascular system, hydrolyses epoxyeicosatrienoic acids (EETs) to their corresponding dihydroxyeicosatrienoic acids (DHETs). We previously showed that endogenous lipid electrophiles adduct within the catalytic domain, inhibiting sEH to lower blood pressure in angiotensin II-induced hypertensive mice. As angiotensin II increases vascular H_2O_2, we explored sEH redox regulation by this oxidant and how this integrates with inhibition by lipid electrophiles to regulate vasotone. Kinetics analyses revealed that H_2O_2 not only increased the specific activity of sEH but increased its affinity for substrate and increased its catalytic efficiency. This oxidative activation was mediated by formation of an intra-disulfide bond between C262 and C264, as determined by mass spectrometry and substantiated by biotin-phenylarsinate and thioredoxin-trapping mutant assays. C262S/264S sEH mutants were resistant to peroxide-induced activation, corroborating the disulfide-activation mechanism. The physiological impact of sEH redox state was determined in isolated arteries and the effect of the pro-oxidant vasopressor angiotensin II on arterial sEH redox state and vasodilatory EETs indexed in mice. Angiotensin II induced the activating intra-disulfide in sEH, causing a decrease in plasma EET/DHET ratios that is consistent with the pressor response to this hormone. Although sEH C262-C264 disulfide formation enhances hydrolysis of vasodilatory EETs, this modification also sensitized sEH to inhibition by lipid electrophiles. This explains why angiotensin II decreases EETs and increases blood pressure, but when lipid electrophiles are also present, that EETs are increased and blood pressure lowered.

Keywords: Redox regulation, oxidation, angiotensin II, disulfide, soluble epoxide hydrolase

Introduction

Soluble epoxide hydrolase (sEH) is distributed widely in tissues and is an important regulator of the cardiovascular system (1). This hydrolase is homodimeric with each monomer consisting of a C-terminal domain with epoxide hydrolase activity and an N-terminal domain (NTD) with phosphatase activity (2, 3). The C-terminal domain catalyzes the hydrolysis of epoxides to their corresponding diols. Epoxy-fatty acids, such as epoxyeicosatrienoic acids (EETs), epoxydocosapentaenoic acids (EpDPEs), α- and γ-epoxyoctadecadienoic acids (α/γ-EpODEs) and epoxyoctadecaenoic acids (EpOMEs) are examples of endogenous substrates of sEH. Among these, EETs are the most studied and are known for their ability to induce vasodilation and decrease blood pressure (BP) (4-8). sEH hydrolyses EETs to their corresponding diols, namely dihydroxyeicosatrienoic acids (DHETs), causing blood pressure to increase. Conversely, inhibition of sEH increases EETs that induce vasodilation, highlighting this enzyme as an important determinant of cardiovascular health and disease (9-15). Inhibitors of sEH offer broad cardiovascular protection, including blockade of

smooth muscle proliferation (16). reduction of atherosclerosis and hypertension (13, 17-21), prevention and regression of cardiac hypertrophy, failure (22-24), and fibrosis (25). sEH is expressed in non-vascular tissues, with its inhibition limiting ischemic damage to the heart (26-31). brain and other organs (32, 33). Similarly, sEH null mice are protected from cardiovascular pathologies (28). On the other hand, genetic alterations that enhance sEH activity are a risk factor for human heart failure (22).

sEH activity was considered to be controlled principally by its expression levels (34). However, we showed sEH activity is inhibited by electrophilic lipids, such as 15-deoxy-$\Delta^{12,14}$-Prostaglandin J_2 (15d-PGJ_2) or nitro-oleic acid (35-37). These endogenous lipid electrophiles bind and covalently adduct within the hydrolase C-terminal domain, inhibiting its catalytic activity to provide post-translational regulation of sEH.

The abundance of EETs is commonly decreased in cardiovascular disease scenarios such as myocardial infarction, hypertension, and diabetes (22, 38, 39). and as mentioned above, polymorphisms that increase hydrolase activity cause heart failure. This decline in EETs is likely causal in the pathogenesis of these conditions, with sEH inhibitors that can increase epoxy-fatty acids providing therapy (40). Cardiovascular disease has been broadly linked, often causally, with oxidative stress. This is notable in the context of this study in which we describe a new mechanism of oxidative activation of sEH that would account for the loss of protective EETs.

Given that hydrogen peroxide (H_2O_2) and lipid peroxides are ubiquitous and commonly mediate signalling to control physiological processes by modulating the redox state of proteins (41, 42). we determined their impact on sEH activity. We were intrigued to find that H_2O_2 oxidized and activated the hydrolase. Consequently, we investigated the molecular basis of this oxidative activation, tested if it occurred in cells and tissues and determined if there was a physiological manifestation of these events. The oxidative activation of sEH was caused by formation of an intra-disulfide bond between C262 and C264. Furthermore, angiotensin II, known for its ability to increase cellular H_2O_2 (43, 44), induced the formation of an activating intra-disulfide bond in mouse tissues, resulting in decreased plasma EET/DHET ratios. Thus, this new mechanism in which sEH is activated by oxidative intra-disulfide bond formation, may at least in part, contribute to the increase in blood pressure caused by angiotensin II. Formation of the disulfide also serves to sensitize sEH to inhibition by lipid electrophiles. This explains why angiotensin II decreases EETs and increases blood pressure, but in contrast, when lipid electrophiles are concomitantly present, EET levels are instead increased, and blood pressure lowered.

Materials and Methods

Recombinant protein production

The sEH full-length protein was cloned into pcDNA3.1D/V5-His-TOPO® vector (Invitrogen) as described earlier (45). It was expressed in HEK293-F cells and purified using Ni^{2+}-IMAC as described earlier (45). Following successful purification, the protein fractions were pooled and the imidazole was removed using desalting spin columns (Zeba, ThermoFisher). The protein was then stored in 50 mM Tris pH 7.5, 300 mM NaCl and then snap frozen in liquid N_2 and stored at -80°C. Single mutants C262S, C264S, C262A and C264A were generated using the Quikchange II XL (Agilent) kit. Primers were designed using the Quikchange Primer Designer online tool. Successful mutagenesis was confirmed by sequencing (Eurofins MWG). The sEH mutants were expressed and purified as above as the WT protein. The sEH C-terminal domain was cloned as described earlier.(45) sEH C-terminal domain C264S mutant were obtained using the Q5® Site-Directed Mutagenesis Kit (NEB) and primers designed using the NEB Changer tool. sEH C-terminal domain WT and mutants were purified as described earlier (45) and stored at -80°C in the same buffer used for the full-length protein. Protein concentration was adjusted according to the theoretical molecular weight and extinction coefficient, obtained using the ProtPARAM ExPASY tool (46).

In vitro **sEH enzymatic assays**

Activity of WT and mutant sEH proteins were measured using a spectrofluorometric method (47). The assay uses the substrate 3-phenyl-cyano(6-methoxy-2-naphthalenyl) methyl ester-2-oxiraneacetic acid (PHOME – Cayman), which is hydrolysed by sEH to generate a fluorescent end-product, 6-methoxy-2-naphtaldehyde (6M2N). Specific activity of the recombinant enzymes was measured as described before.(45) Briefly, full-length protein and C-terminal domain enzymes were diluted with reaction buffer (25 mM TRIS-HCl pH 7.4) to respectively 322 nM and 8 µM, to be then mixed with 10 µM TCEP. For oxidation experiments, full-length protein and C-terminal domain enzymes were oxidized with a final concentration of 1, 10 or 100 µM H_2O_2 or *tert*-butyl hydroperoxide for 10 min at room temperature. A time course determined that a 10 minute pre-treatment with H_2O_2 was optimal in terms of maximally stimulating the hydrolase, as shown in Supplementary Figure 1A. In specific activity measurements, the hydrolase was further diluted in reaction buffer in a black 96-well polystyrene microtiter plate (ThermoFisher) to different final concentrations (full-length protein 1, 2, 4, 5, 8, 10 nM; C-terminal domain 5, 10, 50, 100 and 200 nM), then PHOME (0.25 µM final concentration), freshly prepared in DMSO, was added to the 96-well plate. For Michaelis-Menten kinetic experiments, different substrate concentrations were aliquoted in a black 96-well plate (full-length protein 0.25, 0.5, 1, 5, 10, 100 µM; C-terminal domain 0.25, 0.75, 1.5, 5, 10, 20 µM), to then add full-length protein and C-terminal domain enzymes at a final concentration of respectively 8 nM and 15 nM. Relative fluorescence (RFUs) was monitored at excitation 330 nm / emission 450 nm every min for 15 min using CLARIOstar plate reader (BMG Labtech) or a POLARstar Omega (BMG Labtech). A standard curve using 6M2N was used for quantification purposes as described before

5

(45). IC50 measurements for both full-length protein and C-terminal domain proteins with 15d-PGJ$_2$ or AUDA were performed as detailed before (37), oxidation was induced with a final concentration of 1, 10 or 100 µM H$_2$O$_2$ or *tert*-butyl hydroperoxide for 10 min at room temperature, when required. The readout at 15 min was used to build the IC$_{50}$ curve, fitted with "log(inhibitor) vs. response - variable slope" in GraphPad, and further considered exclusively if R^2 was > 0.9.

Quantification of the covalently modified sEH with biotin-15d-PGJ$_2$

To assess if oxidation affected electrophilic 15d-PGJ$_2$ adducting to sEH, biotinylated-15d-PGJ$_2$ (Cayman) was used in an adaptation of the enzymatic assay method described above. Briefly, full-length protein sEH protein was reduced with 10 µM TCEP on ice for 15 min, then diluted in freshly prepared 25 mM TRIS-HCl pH 7.4 to a final concentration of 322 nM. The proteins were then incubated at room temperature for 10 min with or without H$_2$O$_2$ (final concentration 1 µM), the proteins were then subsequently incubated at room temperature for 30 min with biotinylated-15d-PGJ$_2$ (final concentration 10 µM). Protein samples were then re-suspended with an equal volume of 2x reducing Laemmli SDS sample buffer (total volume 100 µl). Protein samples were loaded and separated by SDS-PAGE using Mini-protean 3 system (Bio-Rad) and transferred to PVDF membranes (Bio-Rad). Blots were incubated with the biotin-antibody (#D5A7, Cell Signaling) diluted 1:1000 in PBS-Tween 5% milk overnight. One hr of incubation with horseradish peroxidase-coupled anti-rabbit (#7074, Cell Signaling) IgG secondary antibody (diluted 1:1000 in PBS-Tween in 5% milk) was used to detect the primary antibody, along with ECL reagent (ThermoFisher).

Cell sEH activity assays

Cells treated with or without H$_2$O$_2$ were harvested and lysed in 0.5% digitonin lysis buffer and centrifuged at 3000 g for 5 min at 4 °C. sEH activity was measured with Cyano(6-methoxy-2-napthalenyl)methyl[(2,3)-3-phenyloxiranyl]methyl ester, carbonic acid (Epoxy Fluor 7, Cayman) as a substrate. Total cell lysates were treated with or without AUDA to a final concentration 50 µM for 15 min at 37 °C to determine the sEH contribution of Epoxy Fluor 7 hydrolysis. Subsequently 10 µM Epoxy Fluor 7 (final concentration) was added and fluorescence measurements made at excitation 330 / emission 465 nm every 2 min for 1 h using a CLARIOstar plate reader (BMG Labtech) at 37 °C. Protein concentration were measured using the bicinchoninic acid assay. A standard curve using 6M2N was used for quantification purposes.

Liquid chromatography-tandem mass spectrometry

100 µg of protein was dissolved in 70% formic acid prepared in UHQ Water. The protein was chemical digested following addition of a few crystals of Cyanogen Bromide (Sigma Aldrich, USA). The reaction was carried out at ambient temperature and in the dark for 5 hr and stopped with the addition of 2 mL of UHQ water. The sample was lyophilised and reconstituted in 100 µL of 50 mM ammonium bicarbonate pH 8.4 and a second digestion was performed with the MS grade Trypsin

Gold (Promega, USA) using a 1:50 enzyme:substrate ratio. The reaction was incubated at 37 °C for 5 hrs and halted by addition of formic acid to a final concentration of 0.5%. The digested samples were analysed using an Acquity H Class UPLC instrument, interfacing though an electrospray ionization (ESI) LockSpray source to a High Definition Mass Spectrometer Synapt G2Si qTof, both from Waters Corporation (Milford, MA, USA). Data were acquired using MassLynx v4.1 (Waters, MA, USA), and processed using UNIFI (Waters, MA, USA)

The LC/ESI-MS was carried out using the following conditions: Column: Waters BEH300 C18 100 mm x 2.1 mm, 1.7 µm, Column Temperature: 60 °C, Flow rate: 0.2 mL/min, Mobile Phase A: MS grade UHQ water, 0.1% Formic Acid, Mobile Phase B: MS grade Acetonitrile, 0.1% Formic Acid, 0-2 min at 5% B, 2-40 to 43%B, 2 min to 80%B and at 80% for 3 min. The samples were acquired in MS^e mode using a collision energy ramp from 25 to 45 eV.

Quantification of epoxyeicosatrienoic acids and dihydroxyeicosatrienoic acids

To extract oxylipins, epoxyeicosatrienoic acids (EETs) and dihydroxyeicosatrienoic acids (DiHETs), from plasma, a sample aliquot of 200 microliters was placed in a glass conical tube containing lyophilised antioxidants and deuterated internal standards. Antioxidants triphenylphosphine (TPP) and butylated hydroxytoluene (BTH) were added, each, at a final concentration of 0.2% v/v. EDTA was also added to a final concentration of 1% w/v. The internal standards, 14,15-EETd11 and 14,15-diHETd11, were added at final concentrations of 50 ng/mL and 5 ng/mL, respectively, and desiccated prior to the addition of plasma. Each plasma sample was diluted with 300 µL of phosphate buffer pH 7.8. Lipids were prepared using a Folch extraction by adding 2 mL of 2:1 Chloroform:Methanol to the diluted plasm, left at room temperature for 10 min, and vortexed vigorously at regular intervals. The organic phase containing the oxylipins was recovered by phase partition follow centrifugation and 1500 g for 10 min and was dried under a stream of nitrogen. 1 mL of 1 M NaOH was added to the dried lipid extract and incubated at 90 °C for 20 min. The solution was acidified with formic acid, and lipids were recovered with 4 mL of Ethyl Acetate. The organic phase separated by phase partitioning following centrifugation at 2500 g for 5 min, dried under a stream of nitrogen, and dissolved in a final volume of 50 µL of methanol.

Separation of EETs and DiHETs was carried out by reverse phase using an Acquity H Class UPLC system (Waters Corporation, Milford, MA, USA), configured with a BEH300 C18,100 mm x 2.1 mm, 1.7 µm column (Waters Corporation, Milford, MA, USA) with a constant flow rate of 0.4 mL/min. Column temperature was set at 40 °C. Mobile phases consisted of deionized water with 0.02% acetic acid (A) and acetonitrile (B). The initial condition set at 50%B ramped to 60%B in 0.1 min, and held for 1 min at 60%B, followed by a 2 min step gradient to 70% B, and again 3 min to 80% B. A negative ion mode was chosen in electrospray ionization mass spectrometry (ESI) for sample analysis. Data were acquired using the High Definition Mass Spectrometer (HDMS) Synapt G2Si qTof, (Waters Corporation, Milford, MA, USA), and MassLynx v4.1 acquisition software (Waters Corporation, Milford, MA, USA), and analysed using UNIFI 1.8 (Waters Corporation, Milford, MA, USA).

Quantification of oxylipins was executed by MRM (multireaction monitoring) in negative ion mode using the following precursor ion > fragment ion transitions:

5(6)EET (*m/z* 319.5>191.2), 5(6)DiHET (*m/z* 337.2>145.1), 8(9)EET *m/z* 319.2>155.1), 8(9)DiHET (*m/z* 337.2>127.1), 11(12)EET (*m/z* 319.2>167.1), 11(12)DiHET (*m/z* 337.2>167.1), 14(15)EET (*m/z* 319.2>219.2), 14(15)DiHET (*m/z* 337.2>207.1), 14(15)EET-d11 (*m/z* 330.5>219.2), 14(15)DiHET-d11 (*m/z* 348.6>207.1).

EETs were quantified by linear regression analysis following the generation of a standard curve containing all EET analytes at concentrations ranging from 0.039 ng/mL to 50 ng/mL, and a fixed amount of EET d11, the internal standard, at a concentration of 50 ng/mL. Similarly, DiHET were quantified using a standard with calibrants in concentrations ranging from 0.039 pg/mL to 5 ng/mL, and the diHET d11 as an internal standard at a fixed concentration of 5 ng/mL.

N-Biotinyl p-aminophenyl arsinic acid (Biotin-PAA) far western

The bespoke synthesis of N-Biotinyl p-aminophenyl arsinic acid (Biotin-PAA) was commissioned to SynInnova Laboratories Inc. Recombinant protein was treated under control conditions, with H_2O_2 (100 or 500 µM), 100 µM DTT or β-mercaptoethanol (5% v/v) for 15 min at room temperature. Protein samples were then re-suspended with an equal volume of 2x non-reducing SDS sample buffer. Protein samples were loaded and separated by SDS-PAGE using Mini-protean 3 system (Bio-Rad) and transferred to PVDF membranes (Bio-Rad). Membranes were blocked for 1 hr at RT in Dilution Buffer from Pierce™ Far-Western Biotinylated Protein:Protein Interaction Kit (Thermo Fisher). Biotin-PAA was diluted to 0.4 mM in Dilution Buffer and incubated with the membrane for 1 hr at RT. The membrane was then washed 6 times with PBS-T and subsequently incubated with Streptavidin-HRP at 1:10,000. Protein bands were visualized on chemiluminescence film (GE Healthcare) following incubation of the membranes with ECL Western Blotting Detection Reagents (Pierce).

C35A thioredoxin trapping mutant

Modified pcDNA3.1+/C plasmids, containing a FLAG tag, with either WT thioredoxin or C35A thioredoxin trapping mutant were purchased from GeneScript. HEK cells were maintained in DMEM with 10% FCS and antibiotics. For treatment of HEK, cells were plated on to 12 well plates. HEK cells were transfected either with WT sEH DNA, C35A TRX DNA, C262A sEH DNA or doubly transfected either with WT sEH and C35A TRX DNA or C262A sEH and C35A TRX DNA using Lipofectamine 2000 (ThermoFisher) following the manufacturer's instructions. 24 hr after transfection the cells were treated with or without auranofin (2.5 µM) for 30 min. Following treatment, the cells were lysed in immunoprecipitation buffer (100 mM Tris pH 7.4, 0.5 % Triton-X100, and supplemented with one complete mini EDTA-free protease inhibitor tablet) and subjected to FLAG immunoprecipitation. Briefly, the lysates were incubated with FLAG-agarose beads (Sigma) for 1 hr on a rotating wheel. After three washes with immunoprecipitation buffer the precipitates were re-suspended in Laemmli SDS sample buffer containing at 95 °C. Protein samples were loaded and

separated by SDS-PAGE (4-20% Mini-Protean® TRX™ Precast Protein Gels, Bio-Rad) using Mini-Protean 3 system (Bio-Rad) and transferred to PVDF membranes (Bio-Rad). Blots were incubated with the sEH antibody (#10010146, Cayman) diluted 1:1000 in PBS-Tween 5% milk overnight. One hr of incubation with horseradish peroxidase-coupled anti-rabbit (#7074, Cell Signaling) IgG secondary antibody (diluted 1:1000 in PBS-Tween in 5% milk) was used to detect the primary antibody, along with ECL reagent (ThermoFisher).

Recombinant protein shifts

100 ng recombinant protein (WT or C262A) was treated with H_2O_2 for 15 min, prior to the addition of non-reducing sample buffer. In some samples reducing agent, β-mercaptoethanol, was added. Protein samples were loaded and separated by SDS-PAGE (as described above), using 10% Mini-Protean® TRX™ Precast Protein Gels (Bio-Rad) run at 90 V for 90 min.

Angiotensin II treatment in mice

All procedures were performed in accordance with the Home Office Guidance on the Operation of the Animals (Scientific Procedures) Act 1986 in UK and were approved by an institutional review committee. Mice were anesthetized and subjected to subcutaneous implantation of osmotic minipumps (model 1007D; Alzet) for delivery of angiotensin II (Sigma) at an infusion rate of 1 mg/kg/day for 7 days.

sEH activity in heart samples

Hearts were rapidly isolated and frozen in liquid nitrogen at the end of the protocol. They were then powdered with a pestle and mortar under liquid nitrogen, which they were then stored in until further analysis. The hearts were homogenised (1 mL of buffer per 100 mg of cardiac tissue) on ice in 100 mM Tris pH 7.4 supplemented with a complete mini EDTA-free protease inhibitor (Roche) using a Polytron tissue grinder. sEH activity was determined as described earlier (36).

sEH quantification and molecular shifts in *in vivo* heart samples

Powdered heart samples were homogenised (1 mL of buffer per 100 mg of cardiac tissue) on ice in 100 mM Tris pH 7.4 supplemented with complete mini EDTA-free protease inhibitor (Roche) using a Polytron tissue grinder. Soluble fractions were prepared from the homogenate by adding Triton-X100 to achieve a final concentration of 1% (v/v), with mixing and incubation on ice for 5 min prior to centrifugation at 25,000 g for 5 min at 4 °C. A sample of the homogenates were re-suspended in an equal volume of 2x non-reducing SDS sample buffer. In some samples reducing agent, β-mercaptoethanol, was added to the sample buffer. Protein samples were loaded and separated by SDS-PAGE as described above.

Myography

9

Thoracic aorta from mice were mounted in a Danish Myo Technology tension myograph, stretched to the optimal pretension condition with Danish Myo Technology normalization module and bathed in Krebs solution at 37 °C with a 95% O_2:5% CO_2 environment. Vasotone measurements were made after wake up with KCl (60 mM) by determining the responses of U46619-contracted (0.1 µM) to cumulatively increasing concentrations of 15d-PGJ$_2$ or H_2O_2. In some experiments, vessels were pre-treated with 1 µM H_2O_2 for 30 min prior to the addition of 15d-PGJ$_2$.

AlloSigMA analysis

AlloSigMA is a structure-based statistical mechanical model tool which calculates the per-residue allosteric free energies (Δg_i) associated with residues perturbation. Per-residue $\Delta g_i > 0$ and $\Delta g_i < 0$ correspond to increased and decreased free energies respectively, associated to allosteric signalling following a perturbation (48, 49). Our analysis was carried out on the AlloSigMA web-server (50) in probing map mode, perturbing C262 and C264 on the X-ray crystal structure of hsEH C-terminal domain (PDB entry code 6I5E) (37). The per-residue Δg_i values above ± 1 standard deviation were reported on the hsEH protein structure in blue and red colour scales to indicate, respectively, stabilised and destabilised residues.

PyMOL and MOLE analyses

Using the sculpting tool in PyMOL Molecular Graphics System 2.0 (Schrödinger, LLC), a disulfide bond between C262 and C264 was modelled into the crystal structure of sEH (PDB entry number 1S8O) (51). The results were analysed and visualised in PyMOL. Using MOLE 2.5, a toolkit for automated location and characterisation of protein cavities (52). the volume of the active site tunnel of oxidized and reduced sEH protein structures was measured. The analysis was performed using probe radius of 5 Å and an interior threshold of 1.1 Å.

Michaelis-Menten modeling

Using the kinetic data generated in experiments above and the Michaelis-Menten equation, we extrapolated these results and generated further data points over a wider range of substrate concentrations and plotted the data using Excel.

COPA analysis

COPA (Cysteine Oxidation Prediction Analysis) is a free internet software program accessible at http://copa.calstatela.edu. Through the analysis of the X-ray crystallography structure coordinates available in the Research Collaboratory for Structural Bioinformatics Proteins Data Bank (RCSB PDB), the software predicts cysteines susceptibility to the formation of disulphide bonds in non-membrane proteins in solution (53). The analysis was herein performed on 26 randomly selected deposited X-ray crystallography structures of sEH (**SI Table 1**), all obtained in highly reducing experimental conditions (> 3 mM DTT).

Table 1: List of crystal coordinate used for the computational analysis in COPA.

PDB	Reference	PDB	Reference	PDB	Reference	PDB	Reference
1S8O	(51)	3I1Y	(54)	4HAI	(55)	3WK7	(56)
1VJ5	(51)	3I28	(54)	4J03	(57)	3WK8	(56)
1ZD2	(58)	3KOO	(59)	4JNC	(60)	3WK9	(56)
1ZD3	(58)	3ANS	(61)	3WK4	(56)	3WKE	(56)
1ZD4	(58)	3ANT	(61)	3WK5	(56)	3WKA	(56)
1ZD5	(58)	3PDC	(62)	3WK6	(56)	3WKB	(56)
3OTQ	(63)	3WKC	(56)				

Protein sequence alignments

Primary sequence alignments of sEH were obtained with ClustalW multiple sequence alignment server (64) and alignment figures were generated using Jalview (65).

Statistical analysis

Results are presented as mean ± standard error of the mean (SEM). Differences between groups were assessed using analysis of variance (ANOVA) followed by a two-tailed unpaired Student's *t*-test or for multiple comparisons a Tukey's post-hoc analysis. Results were considered significant with *p*-values less or equal to 0.05.

Results

sEH is activated upon exposure to H_2O_2

H_2O_2 or *tert*-butyl peroxide significantly increased the specific activity of full length recombinant sEH *in vitro* (**Figure 1A-B**), enhancing its ability to hydrolyse epoxide substrates. However, the increased specific activity was not observed with 1 mM H_2O_2, which may be considered a supraphysiological concentration (Supplementary Figure 1B). Exposing a recombinant C-terminal domain fragment of sEH, the domain responsible for epoxy-fatty acid hydrolysis, to H_2O_2 similarly increased the specific activity of the hydrolase, recapitulating the oxidant-induced activation in the full-length enzyme (**Supplementary Figure 1C**). This is consistent with the increased hydrolase activity being predominantly, if not exclusively, linked to oxidative changes in the C-terminal domain. Pre-treatment of recombinant sEH protein *in vitro* with H_2O_2 or *tert*-butyl hydroperoxide also potentiated the inhibition induced by the physiological inhibitor 15d-PGJ$_2$ (**Figure 1C**). Further analysis using biotin-15d-PGJ$_2$ revealed that more of this electrophile adducted to sEH when there had been a pre-treatment with H_2O_2 (**inset on Figure 1C**). Analysis of full length sEH inhibition by 15d-PGJ$_2$, with or without prior exposure to H_2O_2 or *tert*-butyl hydroperoxide, revealed a significant decrease of the half maximal inhibitory concentration (IC_{50}) upon oxidation. This was demonstrated by the fact that the

11

dose-dependent inhibition of sEH by 15d-PGJ$_2$ was significantly leftward shifted when sEH was pre-treated with either of the peroxide oxidants (**Figure 1D-E**). Thus, when the enzyme is oxidized, a lower concentration of the electrophilic inhibitor is required to obtain the same degree of hydrolase inhibition, indicating that these two mechanisms work synergistically. Essentially 15d-PGJ$_2$ is a more potent inhibitor of oxidized than reduced sEH, an observation that was also made in separate studies with recombinant C-terminal domain protein (**Supplementary Figure 1D**). Interestingly, pre-treatment of full length or C-terminal domain sEH with peroxide did not sensitize the hydrolase to inhibition by the synthetic inhibitor 12-(3-adamantan-1-yl-ureido)-dodecanoic acid (AUDA), indicating that the potentiation of inhibition might be linked to specific binding properties of 15d-PGJ$_2$ (**Figure 1F-G and Supplementary Figure 1E**).

An intra-protein disulfide bond mediates hydrolase activation by H$_2$O$_2$

We reasoned that the activation of sEH by peroxide molecules is likely mediated by the oxidative post-translational modification of one or more of the cysteines within the hydrolase domain. H$_2$O$_2$ can react with protein thiols generating sulfenic acid, which, in turn, can be reduced by adjacent thiols, catalysing the formation of reversible intramolecular disulfide bonds.(66) We performed a bioinformatics analysis with the Cysteine Oxidation Prediction Algorithm (COPA) (67), screening 29 X-ray crystallography structures of sEH previously reported in the RCSB PDB database. This revealed an average distance between C262 and C264 of 4.02 ± 0.10 Å and the algorithm predicted a high likelihood that this cysteine pair can form a disulfide (**Supplementary Figure 1F**).

To investigate if a disulfide, as anticipated, forms under the oxidizing conditions and whether this activates the hydrolase, full length recombinant sEH was reduced with dithiothreitol (DTT) or oxidized by exposure to H$_2$O$_2$ or room air. These sEH preparations were individually chemically digested and analysed by liquid chromatography-tandem mass spectrometry. A peptide corresponding to the expected mass-to-charge ratio (*m/z*) of the peptide containing an intra-disulfide between C262 and C264 was observed in the samples exposed to air without DTT (expected *m/z* = 744.5994; observed *m/z* = 744.5991). The C262-C264 disulfide was confirmed by fragmentation of the peptide and identification of its b and y ions (**Figure 2A**). The oxidized peptide was not observed in the DTT-treated sample (**Figure 2B**), indicating that the disulfide bond occurs as a consequence of oxidation and can be reduced by DTT. In samples treated with H$_2$O$_2$, two peptides with mass-to-charge ratios (*m/z*) that indicate the presence of an intra-disulfide between C262 and C264 were observed (**Supplementary Figure 2A**). These results conclusively demonstrate that a disulfide bond forms between C262 and C264 in sEH as a result of oxidation.

To substantiate the COPA bioinformatics analysis and mass spectrometry findings that indicate sEH can form a disulfide, we performed an N-biotinyl p-aminophenyl arsinic acid (biotin-PAA) binding assay, applying this reporter compound to Western blots containing sEH exposed to reducing or oxidizing conditions. The PAA moiety selectively complexes with proteins with reduced, but not oxidized, vicinal thiols (66) and so can be used to index the redox state of sEH, with the biotin

functionality enabling quantification of binding. Under reducing conditions with DTT or mercaptoethanol, when the vicinal cysteine thiols are in their reduced –SH form, biotin-PAA complexed with sEH and was detected using the western blot overlay method. In contrast, when sEH was air oxidized or exposed to H_2O_2, no signal was detected (**Figure 2C,** upper blot), consistent with oxidative intra-protein disulfide bond formation and adding support to the analysis by mass spectrometry. These samples were analysed on another gel probed with an antibody to sEH (**Figure 2C,** lower blot), confirming that hydrolase protein was present in each sample, including those that did not generate a signal in the biotin-PAA assay. Notably, it became apparent that sEH migrated faster on the gel in the oxidized compared to the reduced form. It is well known that intra-disulfide bond formation can induce such downward gel shifts (66), providing a convenient readout of the thiol-disulfide redox state of sEH. To establish if the gel shift reflected the presence or absence of a C262-C264 intra-disulfide, we compared the gel migration of wild type (WT) sEH or C262A sEH, which cannot form the intra-disulfide, under H_2O_2 oxidizing or DTT reducing conditions. The downward gel shift induced by H_2O_2 in WT sEH was absent in the C262S mutant (**Figure 2D-E**), corroborating oxidation induces an intra-disulfide between C262 and C264 that causes a faster migrating band on non-reducing gels.

Reduction of disulfide-sEH by thioredoxin in cells

In the cellular context, proteins that are regulated by disulfides are typically returned to their reduced -SH state by the disulfide reductase thioredoxin (68). Thioredoxin uses two cysteine residues, namely C32 and C35, to catalyse the reduction of protein disulfide bonds. Thioredoxin C32 undergoes a thiol-disulfide exchange with disulfide-containing targets proteins, becoming covalently conjoined by a disulfide bond. This association is transient as it is rapidly resolved by C35, generating a reduced target protein in exchange for oxidation of thioredoxin (68). C35A thioredoxin is unable to complete this reduction cycle and so becomes trapped on the disulfide-targets proteins that it attempts to reduce. We therefore expressed a C35A HA-thioredoxin-FLAG 'trapping mutant' in HEK cells expressing sEH. The affinity tagged thioredoxin allows its capture and the presence or absence of conjoined sEH to be determined. HEK cells expressing WT sEH or C262A sEH together with C35A thioredoxin were exposed to vehicle or auranofin, a thioredoxin reductase inhibitor that causes disulfide proteins to accumulate and increase their interaction with thioredoxin (69). WT sEH basally interacted with C35A thioredoxin and this was enhanced by treatment with auranofin, events that did not occur in cells expressing C262S sEH (**Figure 2F-G**). These data provide further evidence that sEH forms an intra-protein C262-C264 disulfide. Importantly, it also demonstrates this occurs in cells

13

and is recycled back to the reduced state by thioredoxin, which would return hydrolase activity to basal after oxidative activation.

Impact of disulfide formation on sEH enzyme kinetics

To characterise the impact of oxidation on increasing hydrolase activity, Michaelis-Menten kinetics analyses were performed, comparing the performance of full length recombinant sEH in the reduced or intra-protein disulfide state. H_2O_2 decreased the K_M of sEH for substrate in a concentration-dependant manner, with the maximum decrease being ~4-fold lower than in the reduced hydrolase (**Figure 3A**). This indicates that disulfide-sEH requires less substrate to reach half of the V_{max} of the enzyme. The K_{sp} (k_{cat}/K_M) was also significantly increased, indicating that the catalytic efficiency of the enzyme was enhanced upon formation of the disulfide bond (**Figure 3B**). Oxidation decreased the V_{max}, indicating the hydrolysis rate was decreased (**Supplementary Figure 3A**). Virtually identical results were obtained with the recombinant C-terminal domain protein, again consistent with oxidants enhancing activity by post-translationally modifying cysteines in this domain (**Supplementary Figures 3C, D and E**).

Additionally, using the Michaelis-Menten kinetics curves determined in the experiments described above, we projected how the activity rate of sEH changes over a wide range of substrate concentrations (**Supplementary Figure 3F**). This analysis indicates that oxidation principally increases sEH activity (approximately 2.5-fold) at the lower substrate concentrations tested (inset on **Supplementary Figure 3F**). It is notable that these lower concentrations reflect those that occur physiologically (70). and importantly suggests that oxidation renders sEH capable of hydrolysing endogenous, basal levels of substrates that may otherwise be unable to metabolize efficiently.

Cysteines 262 and 264 are required for oxidative activation of sEH

Based on our findings above, the candidate cysteine residues C262 and C264 were mutated to serine to produce C262S or C264S mutant recombinant enzymes that were purified for activity analysis. The increased sEH activity observed in WT hydrolase upon H_2O_2 treatment was absent in both of the serine mutants (**Figure 3C**). WT or C262S or C264S sEH were also expressed in HEK cells, before exposure to vehicle or H_2O_2 and measuring the impact on hydrolase activity. Again, this demonstrated that the WT sEH activity was increased by H_2O_2 treatment, but was absent in both the serine and alanine mutants that cannot form the activating disulfide when exposed to oxidant (**Figure 3D-E**). These observations are consistent with C262 and C264 being crucial to the peroxide induced activity increase.

The significant decrease in K_M in WT sEH induced by H_2O_2 was also absent in the C262S full-length mutant recombinant protein, though minor decreases in K_M were observed for C264S mutated full-length protein following H_2O_2 treatment, which were not significantly different (**Figure 3A**). There were no significant changes in V_{max} in either C262S or C264S mutated full-length proteins following H_2O_2 treatment (Supplementary Figure 3B). Unlike WT hydrolase, there was no significant change

in the K_M of the C262S sEH mutant following H_2O_2 treatment. An increase in K_{sp} for C264S (**Figure 3B**) was observed, although negligible compared to the large increase induced in the WT by H_2O_2. When the C264 thiol was mutated to a non-reactive serine residue in the C-terminal domain preparation, no significant changes in either K_M, K_{sp} or V_{max} upon oxidation were observed (**Supplementary Figure 3G, H and I**), once again recapitulating the observations made with full-length protein. Altogether, these findings are consistent with C262 and C264 being crucial to the peroxide-induced activity increase, through the formation of the intra-protein disulfide observed in our experiments.

In silico analysis of disulfide bond formation in sEH

To evaluate the effects of disulfide bond formation on the structure of human sEH we performed an AlloSigMA analysis. The software calculates the per-residue allosteric free energy variations (Δg_i) as a consequence of a molecular perturbation, namely a disulfide in this case. In this analysis, residues showing an increase in Δg_i are destabilised and exhibit increased dynamics, and *vice versa* when a decrease in Δg_i is observed (48). This analysis indicated that the catalytic triad was largely unaffected by the formation of the disulfide bond, while the W334 niche of the active site becomes more rigid and the F267 pocket more dynamic (**Figure 4**). The magnitude of the observed Δg_i values would indicate a likely conformational rearrangement of the amino acids forming the surface of the F267 pocket (**Supplementary Figure 4A**), which may presumably enable both substrate and 15d-PGJ$_2$ to accommodate better in the active site. This would account for the enhanced substrate hydrolysis, as well as the potentiated inhibition by 15d-PGJ$_2$ when present, if sEH is oxidised to the disulfide state. We then mimicked a disulfide bond on the reduced X-ray crystallographic structure of human sEH (PDB entry number 1S8O) in PyMOL and used MOLE to measure the active site tunnel volume. This showed there was a general reduction in tunnel volume, from 5533 to 3529 $Å^3$ when the disulfide was present (**Supplementary Figure 4B**). Although our analysis is based only on local atomic geometries optimisation of the structure, this would agree with the AlloSigMA analysis that indicates that the enzyme undergoes a subtle conformational rearrangement that likely enhances the affinity for substrate and inhibitor. Surprisingly, the AlloSigMA analysis indicates a significant increase in the rigidity of the dimer interface (**Figure 4**).

sEH activation *in vivo* contributes to angiotensin II mediated hypertension

We hypothesised that angiotensin II may promote sEH oxidative activation *in vivo* because this vasopressor hormone increases endogenous H_2O_2 via oxidase activation (44, 71). There was a significant increase in sEH expression and activity in the myocardium of mice administered angiotensin II (**Figure 5A-B**). However, the increased activity after angiotensin II exposure was much more than could be accounted for by the increase in sEH expression (**Figure 5C-D**). This is

consistent with another mechanism, namely the oxidative activation of sEH described herein, mediating the increased hydrolase activity.

Consistent with increased sEH activity in mice exposed to angiotensin II, there was a significant decrease in 14,15-EET/DHET and 11,12-EET/DHET ratios in their plasma compared to those that received vehicle (**Figure 5E-F**). In contrast, no significant differences were observed in plasma 5,6- or 8,9-EET/DHET ratios (**Figure 5G-H**). We subsequently measured intra-protein disulfide levels in cardiac tissue of these mice using the non-reducing gel shift assay described above, which showed greater hydrolase oxidation in the angiotensin II group (**Figure 5I-J**). The finding that the vasopressor angiotensin II decreased vasodilatory EETs in plasma is causally consistent with the concomitant disulfide-dependant activation of sEH in these mice.

To investigate this mechanism further, we treated isolated arteries with a low dose of H_2O_2. Aortas were chosen as a model artery because they do not dilate at the H_2O_2 concentration used to induce sEH oxidation, in fact at low doses of H_2O_2 aortas constrict (**Figure 5K**) (72). Whilst resistance arteries are more relevant to blood pressure control, they cannot be used with this protocol because they dilate efficiently to low concentrations of H_2O_2 alone (73). Aortas were pre-treated with H_2O_2 to induce the disulfide in the hydrolase, after which they were exposed to cumulatively increasing concentrations of the physiological sEH inhibitor 15d-PGJ$_2$. This sEH inhibitor relaxes arteries because it increases the abundance of vasodilatory EETs (35). Low dose H_2O_2 induced a minor but statistically significant vasoconstriction as shown in **Figure 5K**. However, when this treatment was combined with 15d-PGJ$_2$, there was a leftward shift in the concentration-response relaxation curve to this lipid (**Figure 5L**). Thus, H_2O_2-induced sensitization of the arterial relaxation to 15d-PGJ$_2$ manifests as a decreased IC$_{50}$ (**Figure 5M**). So, despite starting off more constricted, the aortas dilated more to 15d-PGJ$_2$ when pre-treated with H_2O_2.

This is consistent with our biochemical findings above (**Figure 1**), whereby peroxide also decreased the IC$_{50}$ for sEH inhibition by 15d-PGJ$_2$. The intra-protein disulfide levels in aortas was determined following low dose H_2O_2 treatment by Western blotting. Again, there was a subtle but significant shift in the amount of oxidized sEH form as observed on the Western blot following peroxide treatment, indicating sEH formed the intra-protein disulfide *ex vivo* (**Figure 5N**).

Overall, these results indicate that sEH activation by intra-protein disulfide bond contributes to vasoconstriction and hypertension induced by angiotensin II.

Discussion

Inhibiting sEH attenuates the hydrolytic loss of epoxy-fatty acids, including cyto-protective EETs (11, 12, 20, 24). Consequently, an abundance of pharmacological inhibitors of sEH have been developed (74), with the rationale that they will increase epoxy-fatty acids levels to enable their beneficial actions. sEH is also inhibited by oxidative post-translational modifications, whereby endogenous or

dietary electrophilic lipids adduct to cysteine residues (35, 36), or peroxynitrite nitrates tyrosine residues (75).

Here we report another mechanism of oxidative post-translational regulation in which H_2O_2 induces an intra-protein disulfide bond that activates the hydrolase to decrease EETs. We not only show and characterise this oxidative activation mechanism in detail using recombinant sEH *in vitro* and in cells, but also demonstrate that it operates *in vivo* in mice. The **Graphical abstract** provides a schematic overview of our findings. The observation that sEH can be activated by oxidants is especially notable given the huge investment in developing and testing inhibitors of this hydrolase for therapeutic purposes (76, 77). With these considerations in mind, a logical assertion is that the oxidative activation of sEH is likely to be maladaptive. In the context of cardiovascular disease, increasing sEH activity is considered detrimental and is attributed to loss of protective EETs (13, 20-22). Indeed, oxidative stress has routinely been implicated in the pathogenesis of hypertension. A common explanation for this is oxidative loss of nitric oxide; but the oxidative activation of sEH would provide an additional mechanism. Interestingly, a recent study showed bovine mastitis was associated with a concomitant increase in oxidants and sEH activity (22, 39, 78); consistent with the disulfide activation reported herein.

Our results indicated that sEH activity was increased by oxidation induced by low physiological concentrations of H_2O_2. However, this effect was lost upon exposure to 1 mM H_2O_2, which instead caused some inhibition, as previously observed when similarly high concentrations of oxidants were assessed (79, 80). The bioinformatics analysis showed that C262 and C264 were highly conserved in the phylogenetic tree from *Xenopus tropicalis* to *Homo sapiens*. Interestingly, the amino acids around these cysteines also showed a high degree of homology, consistent with C262 and C264 having important roles in the maintenance of structure or function of sEH, including in humans. Overall, our data indicated that sEH oxidation induced a disulfide bond between C262 and C264. This post-translational modification significantly increased the specific activity and catalytic efficiency of sEH. Our detailed enzymology analysis collectively indicated that oxidation to the disulfide state allows sEH to hydrolytically transform more substrate into product per unit time. Mutation of C262 to serine abrogated the oxidative activation and changes in K_M and K_{sp} observed in WT sEH on exposure to H_2O_2. However, the C264S mutant showed an insignificant trend for the K_M to be decreased and the C264S K_{sp} was significantly increased after H_2O_2 treatment. These alterations in hydrolase performance after exposure to H_2O_2 are minor compared to those in WT and may be because C262 is more oxidant reactive than C264. In this scenario, C262 may react with H_2O_2 to stepwise form a sulfenic acid, which can be further oxidized to sulfinic or sulfonic acid, events that would potentially explain these minor changes in enzyme kinetics. Interestingly, the V_{max} following oxidation also decreased (Supplementary Figures 3A, E, & I), most likely reflecting an increased retention time of the hydrolysis product in the active site of the enzyme. One could envisage that a side chain rearrangement upon oxidation suggested by our molecular modelling data might improve the binding of the hydrolysis product. However, the increased affinity of the substrate (K_M), together

with an improved substrate accommodation in the proximity of the catalytic triad, overcomes the reduced enzymatic turnover and leads to an overall increase in specific activity and catalytic efficiency (Ksp). Using the Michaelis-Menten constants determined for WT sEH, we determined the impact of oxidation on hydrolysis of its substrates at different concentrations as shown in **Supplementary Figure 5**. This analysis illustrates when substrate concentration is below ~1.6 µmol/L, which is typical in biological systems (70), that the impact of oxidation is to increase epoxide hydrolysis. Hence, oxidation to the intra-protein disulfide is a switch that enables sEH to hydrolyse EETs at the levels they occur basally. Although these conclusions are based on studies with the synthetic substrate PHOME, Gomez *et al.* concluded that its hydrolysis is mechanistically similar (i.e. alkyl-enzyme intermediate followed by hydrolytic release) to that of physiological epoxy-fatty acids (58). Thus, the effects of sEH oxidation observed are likely to be recapitulated for the catalysis of biologically relevant substrates. Nevertheless, by lowering the K_M for substrate by inducing the disulfide, oxidants bring EETs within 'range' of the hydrolase. Indeed, in mice exposed to pro-oxidant angiotensin II, in which disulfide-sEH accumulates, there was a decrease in the EETs/DHETs ratio, consistent with the increased sEH activity.

Analysis using AlloSigMA revealed that the intra-protein disulfide bond between C262 and C264 induce a conformational rearrangement of the amino acids that form the surface of the so-called F267 pocket, one of the two sides of the hydrophobic tunnel where the enzyme active site resides. In addition, our data generated with PyMOL and MOLE are consistent with a noticeable narrowing of the F267 pocket when the C262-C264 disulfide bond is present. Overall, this would suggest that the substrate can be stabilised in the active site, optimising its hydrolysis and, thus, increasing the enzyme specific activity. Our previous study showed that the F267 can also accommodate the electrophilic lipid 15d-PGJ$_2$ before it adducts the cysteine residues C521 and C423, inhibiting the enzyme (37). Our modeling would then suggest that, upon formation of the disulfide bond, the 15d-PGJ$_2$ would also bind tighter in this region of the active site, exerting a more effective inhibition as herein observed. Also, this would increase its residency time in the active site and allow a more effective covalent adduction, as here reported.

The finding that thioredoxin reduces disulfide-sEH back to the reduced –SH state in cells means that basal hydrolase activity can be recovered in a regulated manner after oxidative activation. sEH was identified as a substrate for thioredoxin previously (81), again consistent with the disulfide being reversible. However, crystal structures of sEH indicates that the disulfide between C262 and C264 is not on the surface of the protein and so precisely how thioredoxin reduces the disulfide remains unclear. Thioredoxin can reduce buried disulfide bonds in arsenate reductase with the involvement of additional cysteine residues (82), so it is feasible that thioredoxin could do the same to the disulfide in sEH. Confidence that thioredoxin truly reduces the C262-C264 disulfide comes from the fact that C262S sEH was not significantly captured by the trap mutant. In addition, cells exposed to auranofin to inhibit thioredoxin reductase and limit thioredoxin-dependant substrate reduction caused more sEH to be captured with the trap mutant.

We investigated if C262-C264 disulfide-sEH formed *in vivo* and if so whether oxidation event mediated a physiological effect. Angiotensin II is a pro-oxidant peptide hormone that causes arterial constriction, elevating blood pressure in animals and humans (83), it also stimulates NADPH oxidases, producing superoxide and H_2O_2 (43, 84, 85). Consequently, we speculated that angiotensin II may therefore indirectly induce a disulfide bond in sEH, activating the hydrolase. Indeed, angiotensin II induced a disulfide bond within sEH, and increased its activity. These observations are consistent with our biochemical findings in which recombinant sEH *in vitro* or in cells is activated by oxidation.

EETs were decreased in mice exposed to angiotensin II or in models of ischemia-reperfusion, scenarios where oxidant levels are also increased (13, 21, 86, 87), consistent with our findings that oxidation induces activation of sEH. EETs offer several cardiovascular benefits, including reducing blood pressure, attenuating ischemic damage and modulating inflammatory responses. Therefore, an increase in sEH activity due to disulfide bond formation will limit the protective cardiovascular effects of the EETs. Inhibition of sEH offers cardiovascular protection in a variety of different disease scenarios (21, 88), which is consistent with oxidative activation of the hydrolase causally contributing to the pathogenesis of these disease states. In this connection, there are a number of human single-nucleotide polymorphisms (SNPs) in sEH that enhance hydrolase activity and are risk factors for human heart failure (89). Interestingly, the human polymorphism R287Q is capable of disrupting the enzyme dimerization, and reducing *in vitro* epoxy-hydrolytic activity (90). Perhaps enhanced rigidity at the dimerization interface induced by the disulfide bond between C262 and C264, as our AlloSigMA analysis indicated may occur, stabilises the dimer in solution to increase hydrolase activity.

The plasma of angiotensin II treated mice showed significantly decreased 14,15- EET/DHET and 11,12-EET/DHET ratios, consistent with C262-C264 disulfide activation of sEH enhancing hydrolysis of EETs. Interestingly, sEH activation and increased DHET abundance was observed in HEK cells during nitrosative stress and was attributed to S-nitrosation of C264 (38). This is notable, as we have previously shown that S-nitrosated proteins generically transition to disulfide bond formation (91), hence it is likely that the S-nitrosation of C264 induced the activating intra disulfide with C264. In contrast to the increase in 14,15- EET/DHET and 11,12-EET/DHET during angiotensin II treatment, the 8,9- or 5,6-EET/DHET ratios were not altered. sEH has some selectivity towards different EET regioisomers, with 14,15-EET being its preferred substrate, followed by 11,12- and 8,9-EET, with 5,6-EET being considered a poor sEH substrate (92). Of course, formation of the disulfide may changes this substrate selectivity and could account for the 8,9- or 5,6-EET/DHET ratios not changing. Although there are well-established mechanisms of angiotensin II-induced hypertension (93), our observations are consistent with oxidant-induced sEH activation also plays a causal role, although it is difficult to determine the relative contribution of the various mechanisms.

Our observations not only demonstrate that disulfide formation enhances sEH activity, but also shows it sensitizes the hydrolase to inhibition by the electrophilic lipid 15d-PGJ$_2$ when it is present.

19

These results are consistent with the peroxide-induced disulfide causing a conformational change that both enhances utilization of substrates as well as inhibition by 15d-PGJ$_2$, consistent with the structural modeling outlined above. Interestingly, peroxide-induced sensitization was not observed with the inhibitor AUDA. Although a crystal structure of sEH with AUDA bound is not available, the interaction of this inhibitor within the active site may be unaffected by the disulfide, based on its physico-chemical properties. This oxidant-induced sensitization to inhibition by 15d-PGJ$_2$ was recapitulated in isolated arteries, whereby low dose H$_2$O$_2$ pre-treatment enhanced arterial vasodilation to 15d-PGJ$_2$. Thus, despite arteries being slightly more constricted after pre-treatment with low dose H$_2$O$_2$, which could be due to disulfide activation of sEH, their subsequent dilatory responses to 15d-PGJ$_2$ were enhanced compared to those without the initial exposure to oxidant.

In conclusion, sEH activity is redox regulated by the presence or absence of an intra-disulfide bond. Oxidants such as H$_2$O$_2$ induce a C262-C264 intra-disulfide that increases hydrolysis of vasodilatory EETs to cause vasoconstriction and increase blood pressure. Formation of the disulfide lowers the K_M of sEH for its substrates, enabling efficient hydrolysis of the basal levels of EETs. This disulfide-activation mechanism, which occurs *in vivo* in response to the pro-oxidant angiotensin II, may in part account for the pressor effect of this hormone. Formation of the disulfide also serves to sensitize sEH to inhibition by lipid electrophile if they are present. This explains why angiotensin II decreases EETs and increases blood pressure, but when lipid electrophiles are present, EET levels are instead increased and blood pressure lowered. It is conceivable that people who consume a Mediterranean diet, which supplies lipid electrophiles, maintain a normal blood pressure during oxidative stress because of the sEH inhibition mechanism described here.

Acknowledgments

Declaration of competing interest

None of the authors have any conflicts of interest to declare.

References

1.   J. D. Imig, Epoxides and soluble epoxide hydrolase in cardiovascular physiology. *Physiol Rev* **92**, 101-130 (2012).
2.   M. A. Argiriadi, C. Morisseau, B. D. Hammock, D. W. Christianson, Detoxification of environmental mutagens and carcinogens: structure, mechanism, and evolution of liver epoxide hydrolase. *Proc Natl Acad Sci U S A* **96**, 10637-10642 (1999).
3.   J. K. Beetham *et al.*, Gene evolution of epoxide hydrolases and recommended nomenclature. *DNA Cell Biol* **14**, 61-71 (1995).
4.   W. B. Campbell *et al.*, 14,15-Dihydroxyeicosatrienoic acid relaxes bovine coronary arteries by activation of K(Ca) channels. *American journal of physiology. Heart and circulatory physiology* **282**, H1656-1664 (2002).
5.   W. B. Campbell, D. Gebremedhin, P. F. Pratt, D. R. Harder, Identification of epoxyeicosatrienoic acids as endothelium-derived hyperpolarizing factors. *Circ Res* **78**, 415-423 (1996).
6.   W. B. Campbell, D. R. Harder, Endothelium-derived hyperpolarizing factors and vascular cytochrome P450 metabolites of arachidonic acid in the regulation of tone. *Circ Res* **84**, 484-488 (1999).
7.   I. Fleming *et al.*, Epoxyeicosatrienoic acids regulate Trp channel dependent Ca2+ signaling and hyperpolarization in endothelial cells. *Arteriosclerosis, thrombosis, and vascular biology* **27**, 2612-2618 (2007).
8.   A. Luria *et al.*, Compensatory mechanism for homeostatic blood pressure regulation in Ephx2 gene-disrupted mice. *J Biol Chem* **282**, 2891-2898 (2007).
9.   J. D. Imig, B. D. Hammock, Soluble epoxide hydrolase as a therapeutic target for cardiovascular diseases. *Nature reviews. Drug discovery* **8**, 794-805 (2009).
10.   N. Chiamvimonvat, C. M. Ho, H. J. Tsai, B. D. Hammock, The soluble epoxide hydrolase as a pharmaceutical target for hypertension. *Journal of cardiovascular pharmacology* **50**, 225-237 (2007).
11.   J. P. Marino, Jr., Soluble epoxide hydrolase, a target with multiple opportunities for cardiovascular drug discovery. *Curr Top Med Chem* **9**, 452-463 (2009).
12.   J. D. Imig, Cardiovascular therapeutic aspects of soluble epoxide hydrolase inhibitors. *Cardiovasc Drug Rev* **24**, 169-188 (2006).
13.   J. D. Imig *et al.*, An orally active epoxide hydrolase inhibitor lowers blood pressure and provides renal protection in salt-sensitive hypertension. *Hypertension* **46**, 975-981 (2005).
14.   G. J. Gross, K. Nithipatikom, Soluble epoxide hydrolase: a new target for cardioprotection. *Curr Opin Investig Drugs* **10**, 253-258 (2009).
15.   X. Fang, Soluble epoxide hydrolase: a novel target for the treatment of hypertension. *Recent Pat Cardiovasc Drug Discov* **1**, 67-72 (2006).
16.   B. B. Davis *et al.*, Attenuation of vascular smooth muscle cell proliferation by 1-cyclohexyl-3-dodecyl urea is independent of soluble epoxide hydrolase inhibition. *J Pharmacol Exp Ther* **316**, 815-821 (2006).
17.   A. Ulu *et al.*, Soluble epoxide hydrolase inhibitors reduce the development of atherosclerosis in apolipoprotein e-knockout mouse model. *Journal of cardiovascular pharmacology* **52**, 314-323 (2008).
18.   M. Revermann, Pharmacological inhibition of the soluble epoxide hydrolase-from mouse to man. *Curr Opin Pharmacol* **10**, 173-178.
19.   J. J. Olearczyk *et al.*, Administration of a substituted adamantyl urea inhibitor of soluble epoxide hydrolase protects the kidney from damage in hypertensive Goto-Kakizaki rats. *Clin Sci (Lond)* **116**, 61-70 (2009).
20.   O. Jung *et al.*, Soluble epoxide hydrolase is a main effector of angiotensin II-induced hypertension. *Hypertension* **45**, 759-765 (2005).
21.   J. D. Imig, X. Zhao, J. H. Capdevila, C. Morisseau, B. D. Hammock, Soluble epoxide hydrolase inhibition lowers arterial blood pressure in angiotensin II hypertension. *Hypertension* **39**, 690-694 (2002).
22.   J. Monti *et al.*, Soluble epoxide hydrolase is a susceptibility factor for heart failure in a rat model of human disease. *Nat Genet* **40**, 529-537 (2008).

23. T. R. Harris, N. Li, N. Chiamvimonvat, B. D. Hammock, The potential of soluble epoxide hydrolase inhibition in the treatment of cardiac hypertrophy. *Congest Heart Fail* **14**, 219-224 (2008).

24. D. Ai *et al.*, Soluble epoxide hydrolase plays an essential role in angiotensin II-induced cardiac hypertrophy. *Proc Natl Acad Sci U S A* **106**, 564-569 (2009).

25. P. Sirish *et al.*, Unique mechanistic insights into the beneficial effects of soluble epoxide hydrolase inhibitors in the prevention of cardiac fibrosis. *Proc Natl Acad Sci U S A* **110**, 5618-5623 (2013).

26. A. Motoki *et al.*, Soluble epoxide hydrolase inhibition and gene deletion are protective against myocardial ischemia-reperfusion injury in vivo. *American journal of physiology. Heart and circulatory physiology* **295**, H2128-2134 (2008).

27. K. R. Chaudhary, M. Abukhashim, S. H. Hwang, B. D. Hammock, J. M. Seubert, Inhibition of soluble epoxide hydrolase by trans-4-[4-(3-adamantan-1-yl-ureido)-cyclohexyloxy]-benzoic acid (t-AUCB) is protective against ischemia reperfusion injury. *Journal of cardiovascular pharmacology* 10.1097/FJC.0b013e3181c37d69 (2009).

28. J. M. Seubert *et al.*, Role of soluble epoxide hydrolase in postischemic recovery of heart contractile function. *Circ Res* **99**, 442-450 (2006).

29. J. M. Seubert, D. C. Zeldin, K. Nithipatikom, G. J. Gross, Role of epoxyeicosatrienoic acids in protecting the myocardium following ischemia/reperfusion injury. *Prostaglandins Other Lipid Mediat* **82**, 50-59 (2007).

30. N. Li *et al.*, Beneficial effects of soluble epoxide hydrolase inhibitors in myocardial infarction model: Insight gained using metabolomic approaches. *J Mol Cell Cardiol* **47**, 835-845 (2009).

31. M. J. Merkel *et al.*, Inhibition of soluble epoxide hydrolase preserves cardiomyocytes: role of STAT3 signaling. *American journal of physiology. Heart and circulatory physiology* **298**, H679-687.

32. K. W. Sellers *et al.*, Novel mechanism of brain soluble epoxide hydrolase-mediated blood pressure regulation in the spontaneously hypertensive rat. *FASEB J* **19**, 626-628 (2005).

33. M. J. Corenblum *et al.*, Altered soluble epoxide hydrolase gene expression and function and vascular disease risk in the stroke-prone spontaneously hypertensive rat. *Hypertension* **51**, 567-573 (2008).

34. T. R. Harris, B. D. Hammock, Soluble epoxide hydrolase: gene structure, expression and deletion. *Gene* **526**, 61-74 (2013).

35. R. L. Charles *et al.,* Redox regulation of soluble epoxide hydrolase by 15-deoxy-delta-prostaglandin J2 controls coronary hypoxic vasodilation. *Circ Res* **108**, 324-334 (2011).

36. R. L. Charles *et al.*, Protection from hypertension in mice by the Mediterranean diet is mediated by nitro fatty acid inhibition of soluble epoxide hydrolase. *Proc Natl Acad Sci U S A* **111**, 8167-8172 (2014).

37. G. Abis *et al.*, 15-deoxy-Delta(12,14)-Prostaglandin J2 inhibits human soluble epoxide hydrolase by a dual orthosteric and allosteric mechanism. *Commun Biol* **2**, 188 (2019).

38. Y. Ding *et al.*, Soluble epoxide hydrolase activation by S-nitrosation contributes to cardiac ischemia-reperfusion injury. *J Mol Cell Cardiol* **110**, 70-79 (2017).

39. T. Duflot *et al.*, Altered bioavailability of epoxyeicosatrienoic acids is associated with conduit artery endothelial dysfunction in type 2 diabetic patients. *Cardiovasc Diabetol* **18**, 35 (2019).

40. H. C. Shen, B. D. Hammock, Discovery of inhibitors of soluble epoxide hydrolase: a target with multiple potential therapeutic indications. *J Med Chem* **55**, 1789-1808 (2012).

41. A. W. Girotti, Lipid hydroperoxide generation, turnover, and effector action in biological systems. *J Lipid Res* **39**, 1529-1542 (1998).

42. E. A. Veal, A. M. Day, B. A. Morgan, Hydrogen peroxide sensing and signaling. *Mol Cell* **26**, 1-14 (2007).

43. W. J. Welch, Angiotensin II-dependent superoxide: effects on hypertension and vascular dysfunction. *Hypertension* **52**, 51-56 (2008).

44. K. K. Griendling, D. Sorescu, M. Ushio-Fukai, NAD(P)H oxidase: role in cardiovascular biology and disease. *Circ Res* **86**, 494-501 (2000).

45. G. Abis, R. L. Charles, P. Eaton, M. R. Conte, Expression, purification, and characterisation of human soluble Epoxide Hydrolase (hsEH) and of its functional C-terminal domain. *Protein Expr Purif* **153**, 105-113 (2019).

46. C. H. E. Gasteiger, A. Gattiker, S. Duvaud, M.R. Wilkins, R.D. Appel, A. Bairoch, , *The Proteomics Protocols Handbook*. J. M. E. Walker, Ed. (2005), https://doi.org/10.1385/1592598900.

47. N. M. Wolf, C. Morisseau, P. D. Jones, B. Hock, B. D. Hammock, Development of a high-throughput screen for soluble epoxide hydrolase inhibition. *Analytical biochemistry* **355**, 71-80 (2006).

48. E. Guarnera, I. N. Berezovsky, Structure-Based Statistical Mechanical Model Accounts for the Causality and Energetics of Allosteric Communication. *PLoS Comput Biol* **12**, e1004678 (2016).

49. Z. W. Tan, E. Guarnera, W. V. Tee, I. N. Berezovsky, AlloSigMA 2: paving the way to designing allosteric effectors and to exploring allosteric effects of mutations. *Nucleic Acids Res* **48**, W116-W124 (2020).

50. E. Guarnera, Z. W. Tan, Z. Zheng, I. N. Berezovsky, AlloSigMA: allosteric signaling and mutation analysis server. *Bioinformatics* **33**, 3996-3998 (2017).

51. G. A. Gomez, C. Morisseau, B. D. Hammock, D. W. Christianson, Structure of human epoxide hydrolase reveals mechanistic inferences on bifunctional catalysis in epoxide and phosphate ester hydrolysis. *Biochemistry* **43**, 4716-4723 (2004).

52. L. Pravda *et al.*, MOLEonline: a web-based tool for analyzing channels, tunnels and pores (2018 update). *Nucleic Acids Res* **46**, W368-W373 (2018).

53. R. Sanchez, M. Riddle, J. Woo, J. Momand, Prediction of reversibly oxidized protein cysteine thiols using protein structure properties. *Protein Sci* **17**, 473-481 (2008).

54. A. B. Eldrup *et al.*, Structure-based optimization of arylamides as inhibitors of soluble epoxide hydrolase. *J Med Chem* **52**, 5880-5895 (2009).

55. S. Pecic *et al.*, Synthesis and structure-activity relationship of piperidine-derived non-urea soluble epoxide hydrolase inhibitors. *Bioorg Med Chem Lett* **23**, 417-421 (2013).

56. Y. Amano, T. Yamaguchi, E. Tanabe, Structural insights into binding of inhibitors to soluble epoxide hydrolase gained by fragment screening and X-ray crystallography. *Bioorg Med Chem* **22**, 2427-2434 (2014).

57. C. Morisseau, S. Pakhomova, S. H. Hwang, M. E. Newcomer, B. D. Hammock, Inhibition of soluble epoxide hydrolase by fulvestrant and sulfoxides. *Bioorg Med Chem Lett* **23**, 3818-3821 (2013).

58. G. A. Gomez, C. Morisseau, B. D. Hammock, D. W. Christianson, Human soluble epoxide hydrolase: structural basis of inhibition by 4-(3-cyclohexylureido)-carboxylic acids. *Protein Sci* **15**, 58-64 (2006).

59. A. B. Eldrup, F. Soleymanzadeh, N. A. Farrow, A. Kukulka, S. De Lombaert, Optimization of piperidyl-ureas as inhibitors of soluble epoxide hydrolase. *Bioorg Med Chem Lett* **20**, 571-575 (2010).

60. R. K. Thalji *et al.*, Discovery of 1-(1,3,5-triazin-2-yl)piperidine-4-carboxamides as inhibitors of soluble epoxide hydrolase. *Bioorg Med Chem Lett* **23**, 3584-3588 (2013).

61. D. Tanaka *et al.*, A practical use of ligand efficiency indices out of the fragment-based approach: ligand efficiency-guided lead identification of soluble epoxide hydrolase inhibitors. *J Med Chem* **54**, 851-857 (2011).

62. H. Y. Lo *et al.*, Substituted pyrazoles as novel sEH antagonist: investigation of key binding interactions within the catalytic domain. *Bioorg Med Chem Lett* **20**, 6379-6383 (2010).

63. L. Xing *et al.*, Discovery of potent inhibitors of soluble epoxide hydrolase by combinatorial library design and structure-based virtual screening. *J Med Chem* **54**, 1211-1222 (2011).

64. C. Notredame, D. G. Higgins, J. Heringa, T-Coffee: A novel method for fast and accurate multiple sequence alignment. *J Mol Biol* **302**, 205-217 (2000).

65. A. M. Waterhouse, J. B. Procter, D. M. Martin, M. Clamp, G. J. Barton, Jalview Version 2--a multiple sequence alignment editor and analysis workbench. *Bioinformatics* **25**, 1189-1191 (2009).

66. P. Eaton, Protein thiol oxidation in health and disease: Techniques for measuring disulfides and related modifications in complex protein mixtures. *Free Radic.Biol.Med.* **40**, 1889-1899 (2006).

67. H. A. Woo *et al.*, Reduction of cysteine sulfinic acid by sulfiredoxin is specific to 2-cys peroxiredoxins. *J.Biol.Chem.* **280**, 3125-3128 (2005).
68. A. Holmgren, M. Bjornstedt, Thioredoxin and thioredoxin reductase. *Methods Enzymol* **252**, 199-208 (1995).
69. C. Marzano *et al.*, Inhibition of thioredoxin reductase by auranofin induces apoptosis in cisplatin-resistant human ovarian cancer cells. *Free Radic Biol Med* **42**, 872-881 (2007).
70. H. Jiang *et al.*, Identification of 5,6-trans-epoxyeicosatrienoic acid in the phospholipids of red blood cells. *J Biol Chem* **279**, 36412-36418 (2004).
71. D. Ai *et al.*, Angiotensin II up-regulates soluble epoxide hydrolase in vascular endothelium in vitro and in vivo. *Proc Natl Acad Sci U S A* **104**, 9018-9023 (2007).
72. N. Ardanaz, W. H. Beierwaltes, P. J. Pagano, Distinct hydrogen peroxide-induced constriction in multiple mouse arteries: potential influence of vascular polarization. *Pharmacol Rep* **60**, 61-67 (2008).
73. O. Prysyazhna, O. Rudyk, P. Eaton, Single atom substitution in mouse protein kinase G eliminates oxidant sensing to cause hypertension. *Nat Med* **18**, 286-290 (2012).
74. H. C. Shen, Soluble epoxide hydrolase inhibitors: a patent review. *Expert Opin Ther Pat* **20**, 941-956 (2010).
75. E. Barbosa-Sicard *et al.*, Inhibition of the soluble epoxide hydrolase by tyrosine nitration. *J Biol Chem* **284**, 28156-28163 (2009).
76. R. H. Ingraham, R. D. Gless, H. Y. Lo, Soluble epoxide hydrolase inhibitors and their potential for treatment of multiple pathologic conditions. *Curr Med Chem* **18**, 587-603 (2011).
77. C. Morisseau, B. D. Hammock, Impact of soluble epoxide hydrolase and epoxyeicosanoids on human health. *Annu Rev Pharmacol Toxicol* **53**, 37-58 (2013).
78. V. Mavangira *et al.*, Activity of sEH and Oxidant Status during Systemic Bovine Coliform Mastitis. *Antioxidants* **10**, 812 (2021).
79. C. Morisseau, B. L. Ward, D. G. Gilchrist, B. D. Hammock, Multiple epoxide hydrolases in Alternaria alternata f. sp. lycopersici and their relationship to medium composition and host-specific toxin production. *Appl Environ Microbiol* **65**, 2388-2395 (1999).
80. E. C. Dietze *et al.*, Inhibition of human and murine cytosolic epoxide hydrolase by group-selective reagents. *Comp Biochem Physiol B* **104**, 299-308 (1993).
81. L. Weingarten (2008) Identification of novel cytosolic thioredoxin-1 target proteins in mammalian cells by mechanism-basedkinetic trapping.
82. J. Messens *et al.*, How thioredoxin can reduce a buried disulphide bond. *J Mol Biol* **339**, 527-537 (2004).
83. P. K. Mehta, K. K. Griendling, Angiotensin II cell signaling: physiological and pathological effects in the cardiovascular system. *Am J Physiol Cell Physiol* **292**, C82-97 (2007).
84. T. Sousa *et al.*, Role of H(2)O(2) in hypertension, renin-angiotensin system activation and renal medullary disfunction caused by angiotensin II. *Br J Pharmacol* **166**, 2386-2401 (2012).
85. A. M. Zafari *et al.*, Role of NADH/NADPH oxidase-derived H2O2 in angiotensin II-induced vascular hypertrophy. *Hypertension* **32**, 488-495 (1998).
86. C. Zhou *et al.*, Soluble Epoxide Hydrolase Inhibition Protected against Angiotensin II-induced Adventitial Remodeling. *Sci Rep* **7**, 6926 (2017).
87. Z. Cai *et al.*, CYP2J2 overexpression increases EETs and protects against angiotensin II-induced abdominal aortic aneurysm in mice. *J Lipid Res* **54**, 1448-1456 (2013).
88. X. Zhao *et al.*, Soluble epoxide hydrolase inhibition protects the kidney from hypertension-induced damage. *J Am Soc Nephrol* **15**, 1244-1253 (2004).
89. C. R. Lee *et al.*, Genetic variation in soluble epoxide hydrolase (EPHX2) and risk of coronary heart disease: The Atherosclerosis Risk in Communities (ARIC) study. *Hum Mol Genet* **15**, 1640-1649 (2006).
90. J. W. Nelson, R. M. Subrahmanyan, S. A. Summers, X. Xiao, N. J. Alkayed, Soluble epoxide hydrolase dimerization is required for hydrolase activity. *J Biol Chem* **288**, 7697-7703 (2013).
91. K. Wolhuter *et al.*, Evidence against Stable Protein S-Nitrosylation as a Widespread Mechanism of Post-translational Regulation. *Mol Cell* **69**, 438-450 e435 (2018).

92. G. Abis, R. Pacheco-Gomez, T. T. T. Bui, M. R. Conte, Isothermal Titration Calorimetry Enables Rapid Characterization of Enzyme Kinetics and Inhibition for the Human Soluble Epoxide Hydrolase. *Analytical chemistry* **91**, 14865-14872 (2019).
93. S. Higuchi *et al.*, Angiotensin II signal transduction through the AT1 receptor: novel insights into mechanisms and pathophysiology. *Clin Sci (Lond)* **112**, 417-428 (2007).
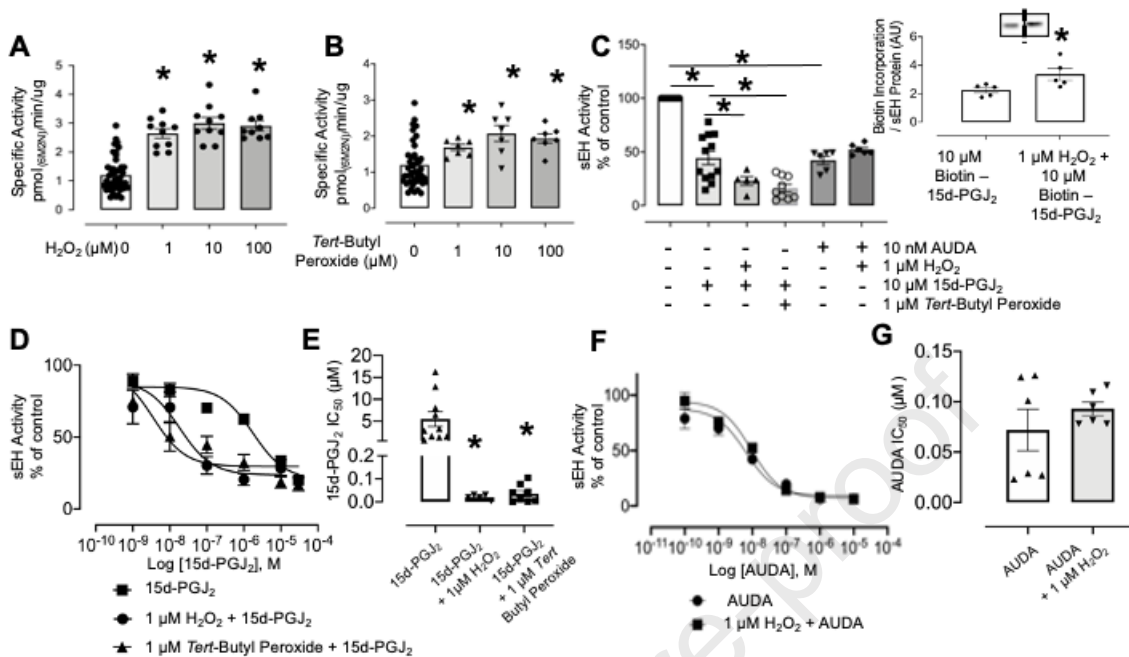
Figures and Tables

Figure 1. The effect of peroxide treatment on sEH activity. (**A**) H_2O_2 increased sEH activity as did (**B**) *tert*-Butyl peroxide. (**C**) H_2O_2 potentiated 15d-PGJ$_2$-dependent inhibition of sEH. H_2O_2 also potentiated adduction of 15d-PGJ$_2$ to sEH as measured by incorporation of a biotin-labelled analogue detected by Western blotting. This potentiation was absent with the par excellence sEH inhibitor, AUDA. Data was normalised to percentage of control. (**D-E**) IC$_{50}$ for 15d-PGJ$_2$-dependent inhibition of hydrolase activity with or without peroxide treatment. Data was normalised to percentage of control. (**F-G**) IC$_{50}$ for AUDA-dependent inhibition of hydrolase activity with or without peroxide treatment. Data was normalised to percentage of control.
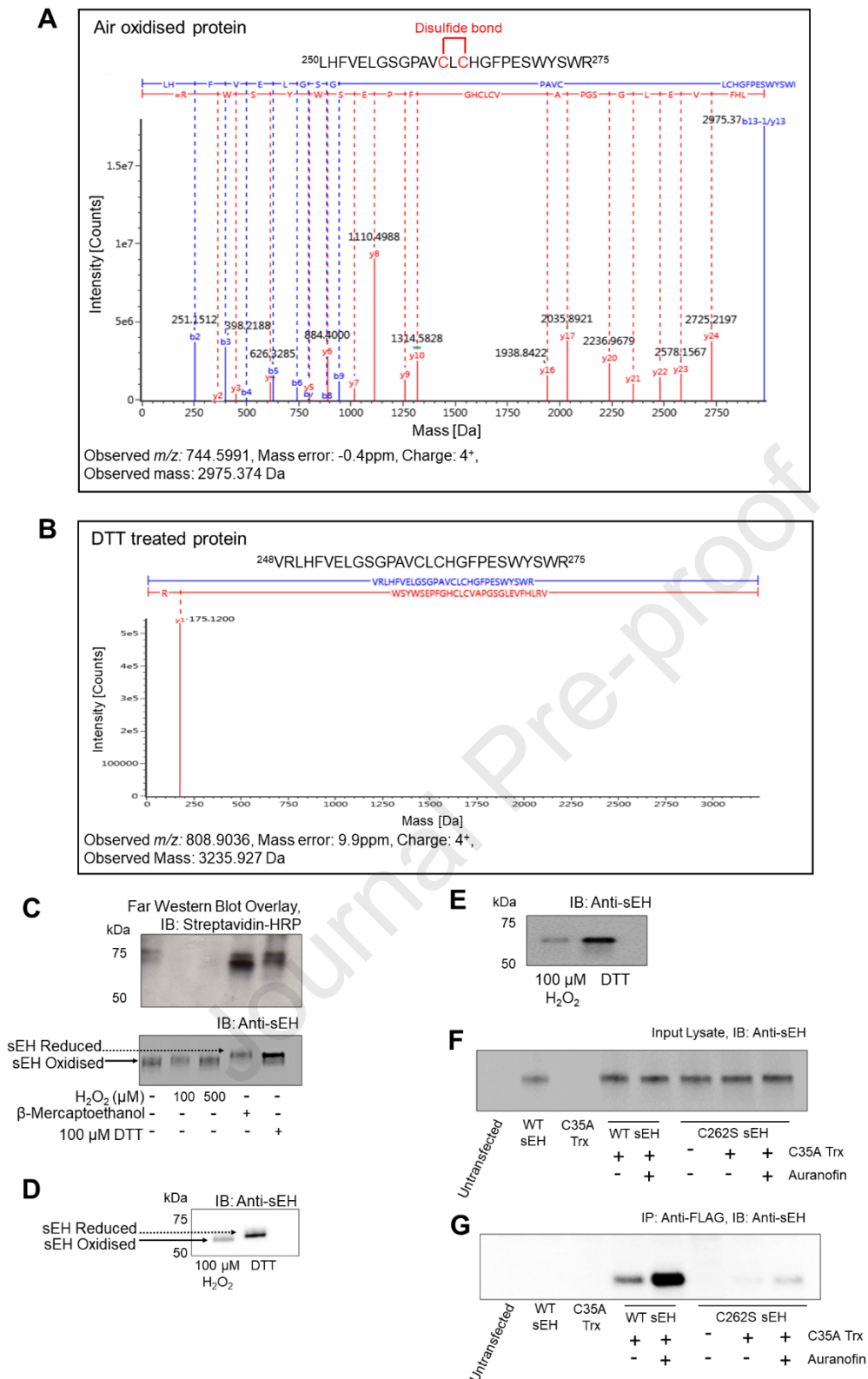
Figure 2. sEH oxidation results in the formation of a disulfide bond. (**A**) An LC-MS/MS spectra identifying a peptide with an *m/z* of 744.5991[4+] (-0.4 ppm) was assigned to the peptide [250]LHFVELGSGPAVCLCHGFPESWYSWR[275] in the air oxidized protein samples. A disulfide bond was detected between the two cysteine residues, C262 and C264, as shown in red. The peptide was confidently assigned through the identification of its b and y ions as shown. (**B**) A peptide with an *m/z* of 808.9036[4+] (9.9 ppm) was identified and assigned to peptide

[248]VRLHFVELGSGPAVCLCHGFPESWYSWR[275], indicating the absence of a disulfide bond as is anticipated when the reductant DTT was present. (**C**) Analysis with biotin-PAA confirmed disulfide bond formation via vicinal thiols within purified recombinant sEH. Following peroxide treatment, biotin-PAA was unable to adduct to sEH, however in reduced samples a band corresponding to sEH was observed when probed with streptavidin-HRP. Western blot below showing that WT sEH protein was present in all lanes following biotin-PAA treatment. This non-reducing blot also showed there was a downwards band shift in sEH when it was exposed to oxidizing conditions. (**D-E**) In separate experiments, recombinant sEH protein samples, which had been exposed to reducing or oxidizing conditions, were probed to monitor for the downwards band shift in sEH. There was a downwards band shift in WT sEH after oxidant exposure, consistent with disulfide formation. In contrast, C262S sEH did not as it does not have the thiols needed to form the disulfide that mediates the shift. (**F**) A C35A Trx trapping mutant was used to identify proteins that form disulfide bonds. Western blot indicating there was equal amounts of sEH in the input for the immunoprecipitation. (**G**) Western blot showing sEH immunoprecipitated from C35A Trx tapping mutant. Following auranofin treatment, a significant amount of WT sEH was captured by the C35A Trx trapping mutant. However, when C262S sEH is used there is significantly less sEH captured by the C35A Trx trapping mutant.
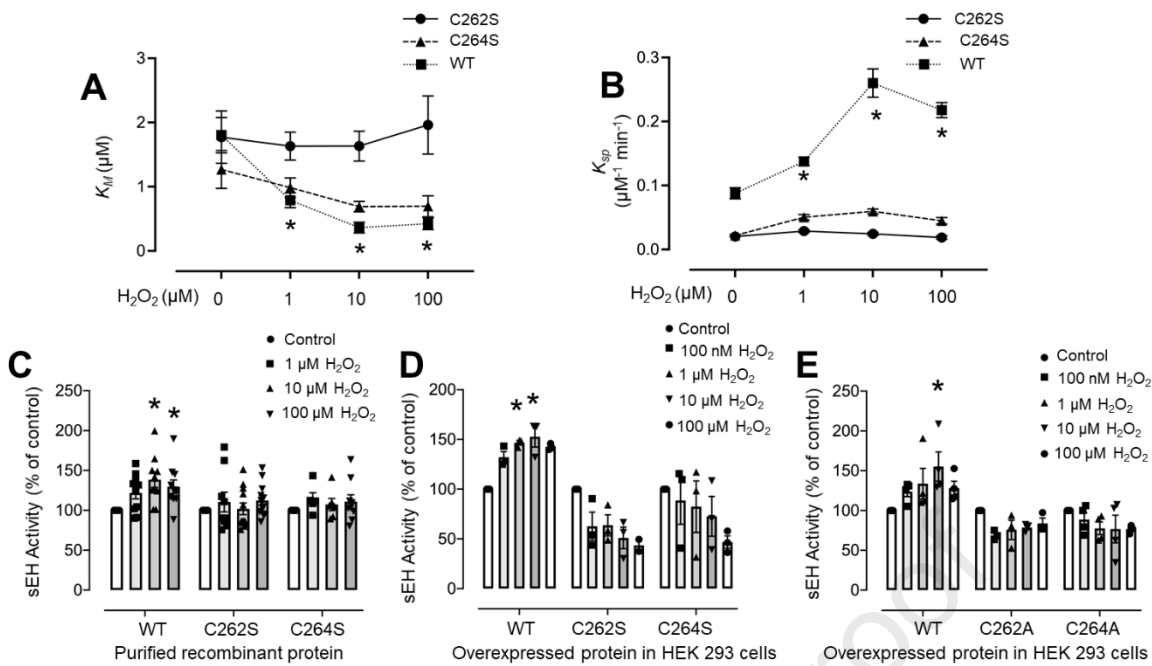
Figure 3. **Enzymatic analysis of sEH**. (**A**) H_2O_2 treatment reduced the K_M of purified recombinant WT sEH, indicating an increased affinity for substrate upon oxidation. No significant changes in K_M was observed for the C262S mutated purified recombinant protein following H_2O_2 treatment. A minor decrease in K_M was observed for the C264S mutated purified recombinant protein following H_2O_2 treatment, which was not significantly different. (**B**) An increase in K_{sp} of recombinant WT sEH was observed following H_2O_2 treatment, indicating an enhanced catalytic efficiency upon oxidation. There was no change in catalytic efficiency (K_{sp}) of C262S following H_2O_2 treatment, however in C264S sEH the K_{sp} was a minor increase. (**C**) The mutation of the thiol moieties of C262 and C264 into non-reactive serine residues abrogated the significant increase in specific activity that was observed with WT sEH recombinant enzyme. Data were normalised to percentage of control. (**D-E**) WT sEH, C262S, C264S, C262A or C264A proteins were overexpressed in HEK cells and their sEH activity was assessed with or without exposure to H_2O_2. There was a significant increase in WT sEH activity following H_2O_2 treatment, which was not observed in cells expressing any of the mutated proteins. Data was normalised to percentage of control.
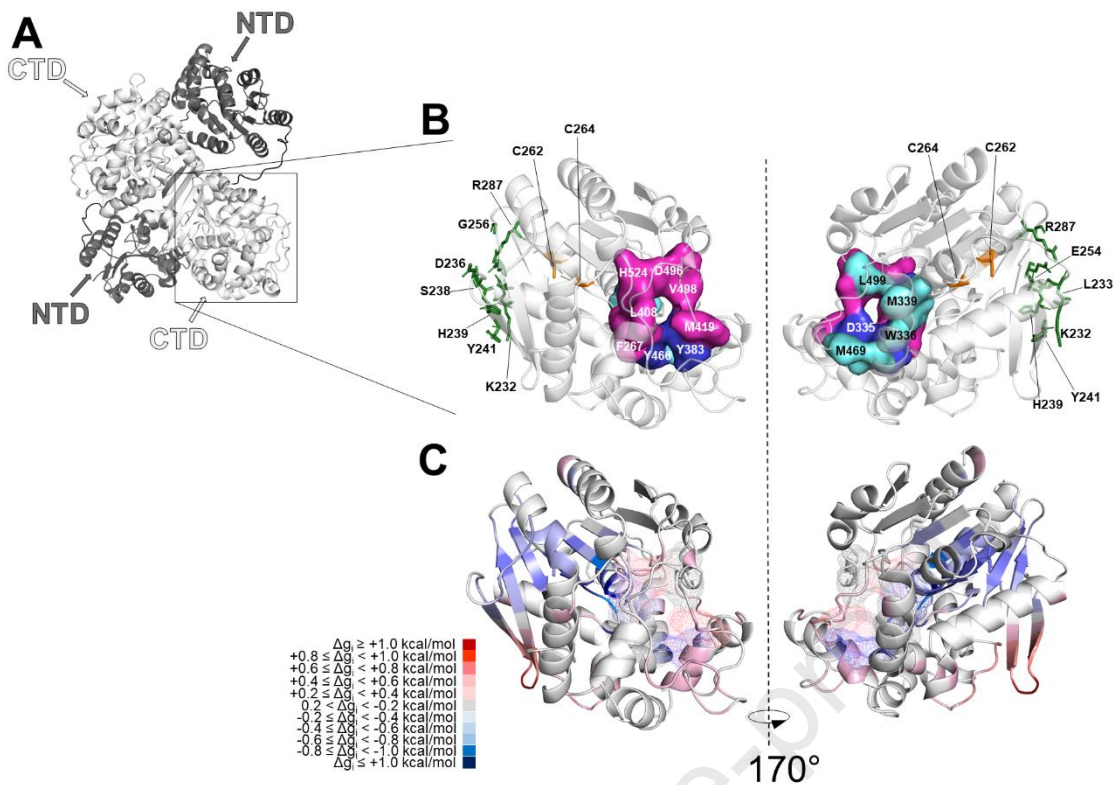
29

Figure 4. **hsEH oxidation might induce conformational rearrangements.** (**A**) sEH is a dimer with a swapped-domain architecture, where the C-terminal domain of one subunit interacts with both the C-terminal domain and the NTD of the other monomeric unit. **(B)** The panel reports the cartoon representation of the structure of hsEH C-terminal domain and its 170° rotation. The 'L-shaped' active site is depicted in surface mode. The F267 pocket, vertex and W334 niche are coloured respectively in magenta, blue and cyan. The cysteine residues involved in the disulfide bond are reported as orange sticks. The residues of the dimerization interface are depicted by green sticks. **(C)** AlloSigMA analysis of the perturbation of C262 and C264. The panel shows a cartoon model of sEH C-terminal domain (same orientations as in **B**), coloured according to the predicted Δg_i. The darker the shade of red or blue, the greater the destabilization or gain in rigidity, respectively.
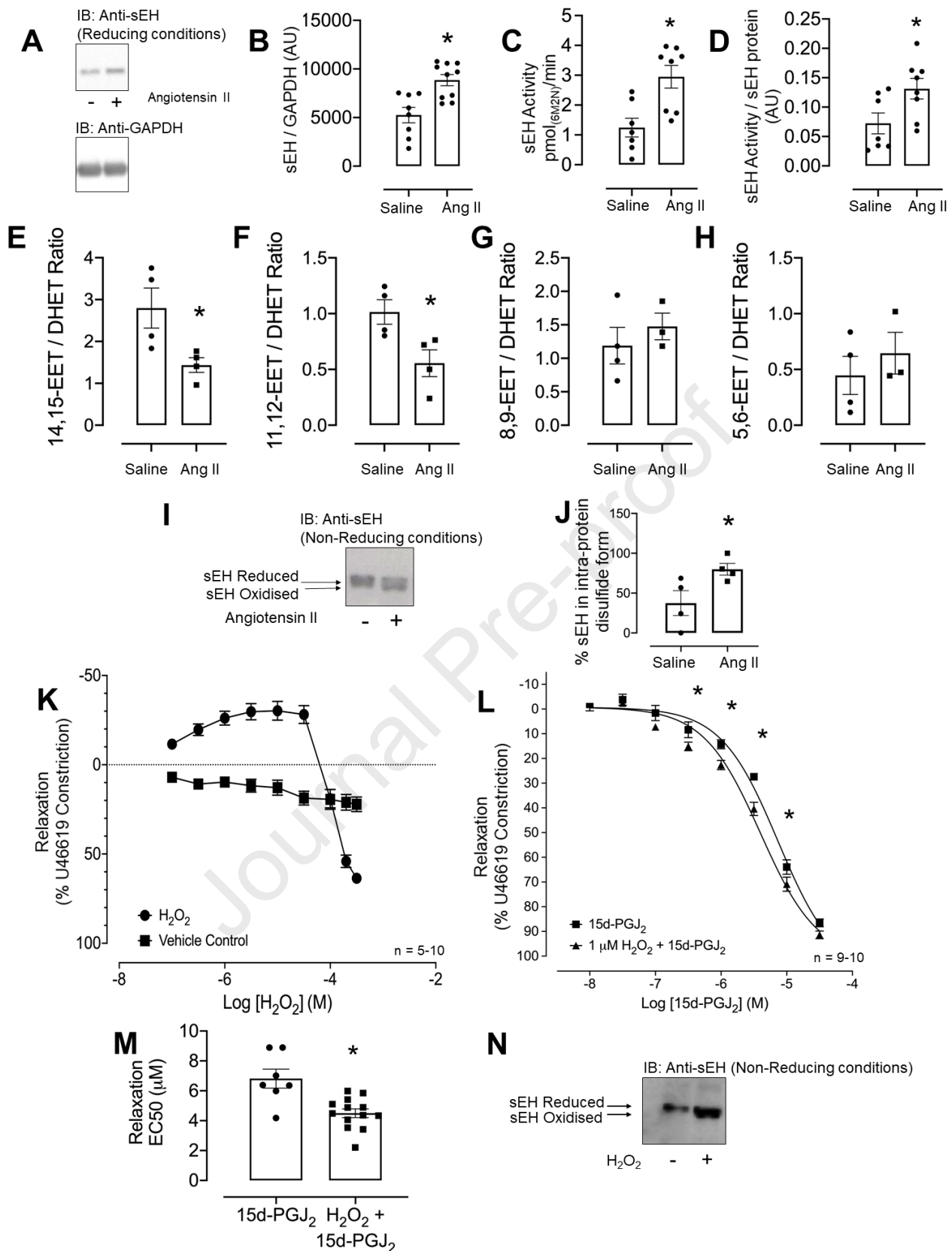
Figure 5. *In vivo* **assessment of novel intra-protein disulfide in sEH.** (**A**) Reducing Western blots showing that angiotensin II induced sEH expression over 7 days. The lower GAPDH blot confirms equal protein loading. (**B**) Angiotensin II treatment significantly increased sEH expression in mouse hearts. (**C**) Angiotensin II treatment significantly increased sEH activity in mouse hearts. (**D**)

31

Correcting hydrolase activity for the increased sEH protein content revealed that hydrolase activity was still significantly increased, consistent with oxidant-induced activation of the hydrolase. (**E-H)** There was a significant decrease in the EET/DHET ratio for 14,15-EET/DHET and 11,12-EET/DHET as compared to saline treatment. No significant differences were observed for the 8,9- or 5,6-EET/DHET ratios. (**I-J**) Non-reducing blot showing there was a downward band shift in sEH in the hearts from angiotensin II treated mice, with quantification shown below, consistent with oxidant–induced disulfide formation. (**K**) H_2O_2 induced constriction of mouse aortas, consistent with sEH activation. (**L-M**) H_2O_2 pre-treatment potentiated 15d-PGJ$_2$-induced arterial dilation, as indicated by the dose-response curve being shifted to the left as compared to the 15d-PGJ$_2$ alone and by the decreased EC50. (**N**) Mouse aortas were assessed for intra-protein disulfide bond formation following peroxide treatment. There was a subtle downwards shift to the faster migrating oxidized form of sEH as shown in the Western blot.

Manuscript Number: REDOX-D-21-00986

A thiol redox sensor in soluble epoxide hydrolase enables oxidative activation by intra-protein disulfide bond formation.

Dear Professor Kevil,

I confirm that the authors do not have any conflicts of interest in connection with this manuscript.

Yours sincerely,

Philip Eaton

Philip Eaton

Thursday, 12 August 2021